LEGIBILITY NOTICE

A major purpose of the Technical Information Center is to provide the broadest dissemination possible of information contained in DOE's Research and Development Reports to business, industry, the academic community, and federal, state and local governments.

Although a small portion of this report is not reproducible, it is being made available to expedite the availability of information on the research discussed herein.

LA-UR-87-3046
(Final)

CONF-8709110--13

LA-UR--87-3046

DE88 003146

Los Alamos National Laboratory is operated by the University of California for the United States Department of Energy under contract W-7405-ENG-36

TITLE: EMITTANCE STUDIES AT THE LOS ALAMOS NATIONAL LABORATORY FREE-ELECTRON LASER

AUTHOR(S): B. E. Carlsten, AT-7, D. W. Feldman, AT-7, A. Lumpkin, P-15, W. E. Stein, AT-7, J. E. Sollid, CLS-8, and R. W. Warren, AT-7

SUBMITTED TO: Ninth International FEL Conference, Williamsburg, Virginia September 14-18, 1987

DISCLAIMER

Los Alamos Los Alamos Natic
Los Alamos, New

FORM NO 836 R4
ST NO 2629 5/81

EMITTANCE STUDIES AT THE LOS ALAMOS NATIONAL LABORATORY FREE-ELECTRON LASER*

B. E. CARLSTEN, MS-H829, D. W. FELDMAN, A. H. LUMPKIN, J. E. SOLLID, W. E. STEIN, and R. W. WARREN

Los Alamos National Laboratory, Los Alamos, NM 87545

Recent emittance studies at the Los Alamos FEL have indicated several areas of concern in the linac and beamline feeding the wiggler. These studies included both experimental measurements and computer simulations. The beamline starts with a 5-A micropulse from the thermionic cathode in the gun. After bunching by velocity modulation and acceleration to 20 MeV in a 1300-MHz standing wave accelerator, the beam current is roughly 250 A. Final bunching to 800 A is performed in the nonisochronous bend that rotates the electrons onto the axis of the wiggler and the optical cavity.

Four emittance growth mechanisms of special importance have been studied. First, a rapid growth of the electron beam's emittance immediately after the spherical gridded Pierce gun resulted, in part, from the long time required for our pulsing electronics to ramp the grid voltage up at the start and down at the end of the pulse, which created a pulse with a cosine-like current distribution as a function of time. The growth was compounded by the extremely small radial beam size (almost a waist) leaving the gun. In addition, we saw evidence of electrostatic charging of the insulators in the gun, reducing the quality of the electron beam further. Second, the action of the solenoidal focusing fields in the low-voltage bunching region was studied, and criteria for a minimum emittance growth were established. Third, maximum misalignment angles and displacements for various elements of the beamline were calculated for the desired low emittance growth. Finally, emittance growth in the horizontal dimension through the nonisochronous bend caused by varying energy depression on the particles due to longitudinal wake fields was both calculated and observed. In addition, we measured energy depressions caused by the wake fields generated by various other elements in the beamline. Strategies were developed to relieve the magnitude of these wake-field effects.

*Work performed under the auspices of the U.S. Department of Energy and the U.S. Army Strategic Defense Command.

1. Introduction

Large unpredicted electron beam emittance at the Los Alamos FEL prompted an experimental study as to its origin. Simultaneously, computer simulations were done to help interpret the findings, which are discussed here.

The paper is divided into three sections. First, an outline of the experiment is given, which includes a description of the beamline elements and techniques used to determine the beam emittance. Second, a summary is given of the experimental results. Emittance measurements were made both before and after our nonisochronous 60° bend; longitudinal wake-field measurements were made at the end of the beamline. The last section contains the discussion of these results, including help in their interpretation from the computer modeling.

2. Outline of experiment

The experimental setup is shown in fig. 1. The main elements are the electron gun, velocity bunching drift region, rf standing wave accelerators, 60° bend, wiggler, and spectrometer.

The electron gun, designed by Litton Industries [1], is pulsed at 21 MHz within a 100-μs macropulse. The pulse length is usually about 3 ns FWHM and the total charge can vary from zero to 15 nC. The current distribution as a function of time is shown in fig. 2. The gun is gridded and is designed to operate at 5 A. It uses a post acceleration anode at 80 kV (fig. 3). After it leaves the gun, the expanding beam then encounters a set of two magnetic lenses L1 and L2, used to focus and match the beam into a drift region surrounded by solenoids in which there is a subharmonic buncher operating at 108 MHz. The peak voltage on the buncher is nominally 60 kV and is used to velocity modulate the beam. Particle overtaking occurs in the ensuing drift region (still surrounded by solenoids), and the peak current is increased by a factor of 30 by the time the bunch reaches the start of the fundamental buncher. The fundamental buncher is operated at 1300 MHz and nominally with a voltage of 1 MeV. Additional particle bunching occurs in this short cavity, and the peak current becomes 50 times the starting value by the time the bunch reaches the first accelerator.

Accelerator tank A (fig. 1) is operated at 1300 MHz and accelerates the beam to 10 MeV. The cells are all side coupled together, but the overall phase can be adjusted for maximum bunching. Particle energy-phase diagrams from simulations using the code PARMELA are shown in fig. 4 to indicate more completely the phase-space dynamics of the longitudinal bunching described above.

After leaving accelerator tank A, the beam is focused by the first quadrupole triplet Q1 through the second accelerator tank, tank B. The beam is accelerated to 20 MeV in tank B and is next focused by the second quadrupole triplet Q2.

The electron bunch is horizontally bent 60° to align it along the optical axis of the wiggler (fig. 5). The bend is achromatic but not isochronous. Thus, if the phase of tank B is adjusted correctly, so-called magnetic bunching can take place in the bend and another factor of 3 enhancement in peak current is possible (fig. 6). After the bend, the bunch can be focused by the third quadrupole triplet Q3 to a waist in the middle of the wiggler.

Quartz (fused silica) screens were available at several positions (fig. 1). In particular there was one after the triplet Q1, two after Q2, and two after Q3. The second screens after Q2 and Q3 were placed about 1 m behind the first. In addition, there were three screens available inside the wiggler. Also between the lenses L1 and L2, just after the electron gun at location 0, we could insert a ruby screen. The predominate light-generating mechanism for the quartz screens is Cherenkov radiation as the beam passes through the material; for the ruby screen it is fluorescence. The Cherenkov light is linear with respect to electron current. A mirror (fig. 7) is used to reflect the light to a TV camera; when the screen data are digitized, they give a reliable description of the transverse current density profile.

Emittance measurements were made using two techniques. First, measurements on the electron beam's transverse size FWHM on any of the quartz screens for various settings of the immediately preceding quadrupole triplet could be made. The data could then be fit with a least squares fitting routine to an ellipse with the appropriate Twiss values, and the emittance could then be calculated. This is a well-known and common technique [2]. As a check, a two-screen measurement can be made. Here, the beam is focused to the smallest possible spot on one screen. Assuming that the beam waist is sufficiently close to that screen (a good assumption for our cases), then the emittance is given by

$$\varepsilon = 4\beta\gamma \frac{D_1 \sqrt{D_2^2 - D_1^2}\ \pi}{4s} ,$$

where D_1 is the beam spot FWHM on the screen near the waist, D_2 is the beam spot FWHM at the second screen, and s is the screens' separation. The factor of $4\beta\gamma$ converts this into the 90% normalized emittance, which we will use throughout this paper. In general only the horizontal emittance was measured, because no growth in the vertical emittance through the 60° bend was found.

After the electron beam leaves the wiggler, it is bent by a spectrometer magnet (fig. 1). In this experiment, the spectrometer was used more to determine the size of wake fields than to find the energy spread inherent in the electron beam. While varying the phase of accelerator tank B (and thus also varying the bunch's time length from 10 to 40 ps), we were able to compare the actual energy of the electron bunch to the sinusoidal curve of the rf fields. The difference in the two curves is a good measurement of the energy droop caused by the wake fields as the bunch's current is peaked.

In addition, transverse rf deflectors operating at 1300 MHz (so-called fast deflectors) can be installed before the screen positions 2 and 4 (fig. 1). These devices allow us both an accurate time measurement of the length of the bunch (to 2 ps) and also allow us to see if different parts of the bunch in time are focused differently. Measurements of the total charge in a pulse were made with a wall-current monitor.

3. Experimental results

The experimental results are in three groups:

(1) Emittance measurements before the 60° bend.

(2) Horizontal emittance measurements after the 60° bend (primarily studying emittance growth in the bend).

(3) Wake-field energy depression measurements.

Evidence was seen of the beam electrically charging the gun's insulators. The beam would be suddenly transversely deflected, and just as suddenly it would come back (the macropulse repetition rate is 1 Hz). The results outlined below are from periods when there was no charging. To more fully understand certain phenomena,

it was desirable to minimize random sources of emittance growth. Thus, the results below are taken with the best selection of lens, solenoid, and quadrupole triplet settings. The emittance measurements are accurate to, at best, 50 π·mm·mrad. Within that uncertainty, there was no noticeable difference between macropulse and micropulse measurements. In addition, variations up to 100 π·mm·mrad in the measurements were observed because of slight differences in the beam transport.

3.1. Emittance measurements before 60° bend

3.1.1. Installation of a 4-mm aperture at location 0 between L1 and L2

At most, 43% of the electrons at the center of the pulse (initially 4 A) can be focused through the aperture. At the optimum focusing for the center, less of the edge electrons get through (fig. 8). As the peak current is reduced, a higher and higher percentage can be transmitted through the aperture.

3.1.2. Installation of a ruby screen at location 0 between L1 and L2

At low peak currents (< 1 A) from the gun, the grid pattern is reproduced on the screen (hence all parts of the micropulse are focused identically) (fig. 9). As the peak current is increased, the electrons are drawn in and the spot size decreases, leaving small radial lines on the periphery of the focal spot and destroying the focal resolution near the center of the spot. Optical effects responsible for the reduction in resolution will be discussed in the next section.

3.1.3. Emittance at quartz screen locations 2 and 3

$\epsilon_{n,\,90\%}$ = 200 π·mm·mrad independent of peak current.

3.2. Emittance measurements after 60° bend

The dominant emittance growth in the horizontal dimension mechanism in the 60° bend has been analytically predicted [3] to be the longitudinal wake fields inside the bend destroying its achromaticity. These predictions were experimentally

verified. The effect of the longitudinal wake fields inside the bend are different for different particles. Some are decelerated the full voltage of the wake fields, and others that are not at the peak of the pulse are decelerated a lesser amount. Because this occurs after the beam is bent by the first dipole but before it is bent by the last one, the bend loses its achromaticity, thus there is emittance growth. One simplistic physical picture of the wake-field mechanism can be made by following the wall currents from the beam. We can see the bend in fig. 10, with an outlet pipe in the third dipole to let the laser light out (the laser is an oscillator). As the wall currents go through the bend, some are lost at the discontinuity caused by the pipe. These wall currents act as an antenna and radiate wake fields. One experimental test is to steer the beam in the bend close to and further away from the hole. As the beam moves closer to the hole, a larger percentage of the wall current passes by the discontinuity and the wake fields should be larger.

3.2.1. Horizontal emittance at quartz screen locations 4 and 5 with 2.5-cm hole in the beam pipe at the downstream dipole

$\varepsilon_{n,\,90\%}$

Beam steered in pipe:	Bunched (400 A) (π·mm·mrad)	Unbunched (100 A) (π·mm·mrad)
Next to hole	900	350
In center of pipe	650	350
Away from hole	500	350

The beam was steered either to or away from the hole until the beam began to scrape the sides of the pipe. Fig. 10 shows the relative sizes of the beam (about 1-cm diameter), beam pipe (4.5-cm diameter) and pipe hole (2.5-cm diameter).

Fig. 11 shows the effect of the wake fields in the bend. The peak current and bunch length can be adjusted by varying the phase of accelerator tank B. As the peak current increases, the beam clearly spreads out in the x-direction, indicating an emittance growth. Fig. 11a corresponds to a bunch length of 45 ps and 11d to 10 ps.

3.2.2. Horizontal emittance at quartz screen locations 4 and 5 with smooth pipe in 60° bend

$\varepsilon_{n,\,90\%}$ = 350 π·mm·mrad (independent of peak current up to 800 A).

With no hole for the outlet pipe, no wake fields are produced.

Placement of the hole at the first upstream dipole appeared to have no effect on the emittance. The TBCI code simulations show that wake fields produced with the hole facing upstream are much lower than with the hole facing downstream.

3.2.3. Horizontal Emittance at quartz screen locations 4 and 5 with large beam pipe (4.5 × 25 cm) and with usual 2.5-cm-hole in the beam pipe at the downstream dipole

$\varepsilon_{n,\,90\%}$ = 300 π·mm·mrad (independent of peak current up to 500 A)

With the large beam pipe, a very small percentage of the wall currents pass near the hole.

3.3. Wake-field energy depression

Energy depression measurements as those described above have led to the following list [4]. Accuracy of the measurements is about 50%. These effects add linearly.

(1) Bellows: 40-keV energy spread per 100-A beam current.

(2) Spectrometer: 60-keV energy spread per 100-A beam current.

(3) Fast deflector: 20-keV energy spread per 100-A beam current.

(4) Pipe discontinuity: 20-keV energy spread per 100-A beam current.

(5) Wiggler without internal beam pipe (magnet structure exposed to beam): 400-keV energy spread per 100-A beam current.

4. Interpretation and comparison with computer simulations

Computer simulations of various parts of the beamline can help us interpret the results discussed in the last section. Most of the simulations were done with the particle-pushing code PARMELA. PARMELA calculates for each particle the magnetic, rf cavity, and space-charge fields present at its location. The Lorentz force equation then prescribes the particle's motion for the next time step. Matrix multiplication of the particle's position and velocity vector is used to determine edge effects of bends, lenses, and solenoids.

The gun can be simulated by the Stanford Linear Accelerator Center (SLAC) Electron Trajectory Program (EGUN) without including the gun's grid, because the grid does not cause significant defocusing of the beam (as we saw in fig. 9).

First, several runs of EGUN are done varying the constants in Child's law, which the program uses to determine cathode emission. This technique simulates the effect of the grid in suppressing the gun's perveance. Final particle trajectory data are saved from each run. Then when PARMELA sets up its input, it can interpolate its particle positions and velocities from that data, needing only the addition of the correct current versus time distribution from fig. 2.

Calculated in this manner, the initial emittance of the gun is quite small, about 15 π·mm·mrad. The initial beam's phase space and longitudinal profile are shown in fig. 12. This beam size is in good agreement with pepper-pot measurements taken in the center of the solenoid region.

However, the beam leaves the gun near a waist and expands radially as it travels to the lenses. There is significant emittance growth in this region because, first, the longitudinal ends of the bunch are radially larger than the center and also because there is less space charge in the ends. As a result, the particles in the center see a tremendously larger radial electric space-charge field than the particles at the ends. The emittance growth scales linearly with the space-charge fields [5] and, thus, is magnified by the small beam size at the center of the bunch. Because of this mechanism, the emittance grows to nearly 60 π·mm·mrad by the time the beam reaches the solenoid region. When we focus the beam through the 4-mm aperture with PARMELA, we see fair agreement with the measurement.

Additional growth to 120 π·mm·mrad is seen by the time accelerator tank A is entered by the particles. The mechanism for emittance growth in the solenoid region is similar in nature, although with the axial magnetic field the exact

dynamics is more complicated. Because of velocity modulation from the subharmonic buncher and the difference in current density along the bunch, the appropriate Brillouin field for the center of the bunch (the cathode is in a field-free region) is not appropriate for the rest of the bunch. If the velocity modulation effect dominates, then the rear of the bunch is overfocused and the front is underfocused [6]. If the velocity modulation is small, then both longitudinal ends are overfocused. In our situation, there is the additional problem of the large variation in radial velocity for the different sections of the beam. The variation of the edge of the beam obeys this equation [7] (if the beam is laminar):

$$\frac{d^2r}{dz^2} + \frac{e}{8mV_o} B_z^2 r - \frac{1}{4\pi\varepsilon_o \sqrt{\frac{2e}{m}} V_o^{3/2} r} = 0 ,$$

where e and m are the electronic charge and mass, V_0 is the beam's voltage, and the applied axial magnetic field is B_z. This equation does not represent simple harmonic motion and indeed the array of different radial velocities from the different radial space-charge forces along the bunch causes scalloping that goes out of phase, causing emittance growth.

The emittance growth is minimized when the beam is kept as parallel as possible in the solenoid region. Emittance growth increases of factors of 2 or more are easily attained if the magnetic field of the front matching section is varied by only 20% because of the above effect.

Experimentally, it was found that diagnostic quartz screens were required everywhere along the solenoid region. We did not have enough diagnostic stations; therefore, the solenoids can only be tuned by trying to infer the emittance downstream. We did this by actually peaking the beam current measured in wall-current monitors after some beam interception took place because of the emittance. Although this technique is not perfect, it probably leads to settings close enough to the optimum.

Misalignment tolerances for the gun, lenses, solenoids, and accelerators were calculated using PARMELA. Maximum transverse offsets and tilts were calculated to keep the emittance growth less than 100 π·mm·mrad. Care was taken to set up the experiment to ensure these tolerances [8].

	Maximum offset (mm)	Maximum tilt angle (mrad)
Gun	1	3
Lens	1	3
Solenoid	2	3
Accelerator	2	3

Even with the perfectly aligned acccelerator tanks, PARMELA predicted the emittance to grow about 150 π·mm·mrad by the end of tank A and 200 π by the end of tank B, in excellent agreement with experiment. Although the space-charge forces were now small, the beam in the tanks had a large enough emittance that the focusing in front of the accelerators could not keep the beam's radial size small inside the tanks. As a result, the time-varying radial rf forces caused more emittance growth.

Horizontal emittance growth from misalignments in the 60° bend had been analytically studied previously [3]. First, a list, reproduced below, was formed that outlined the emittance growth caused by various misalignments in the bend. Referring to fig. 5: D1, D2, and D3 are the labels for the first, second, and third dipoles in the bend. In the list, a number in parenthesis after a dipole label refers to the angle it actually bends the beam. For example D1 (60) means the first dipole bends the beam 60°. The last three entries in the list refer to the cases in which the dipoles are cocked so the beam is bent out of the plane of the beamline (fig. 1). These calculations, using PARMELA, were done with a beam of initial emittance 60 π·mm·mrad. The magnitude of all the errors assumed for these calculations is suspected to be much larger than the actual misalignments.

Effects caused by the energy-independent radial space-charge force [9] in the bend were also calculated. With a 1-cm-diam beam size through the bend and peak currents of 400 A, the emittance would grow to ~250 π·mm·mrad.

Finally, the emittance growth in the bend caused by wake fields is understood. From the earlier study and using the 1-cm-diam beam sizes seen in the bend, the emittance present with the beam steered through the center of the pipe in the bend would correspond to a maximum energy depression of 0.4%. This depression is consistent with the measured value for a pipe discontinuity at 400 A of peak current.

Error	Change in emittance (π·mm·mrad)
Both beam drifts are 2.5 cm longer	1.2
First beam drift is 2.5 cm longer	16.
D1(59), D2(58), D3(59)	14.
D1(59), D2(60), D3(61)	56.8
D1(60), D2(59), D3(59)	47.2
D1(59), D2(59), D3(60)	53.6
First dipole rotated 1° clockwise	44.
Second dipole rotated 1° clockwise	64.4
Third dipole rotated 1° clockwise	56.
First dipole raised 5° out of plane	50.4
Second dipole raised 5° out of plane	44.
Third dipole raised 5° out of plane	44.8

5. Conclusions

The major conclusion of our study is that wake fields were the major emittance growth mechanism and are extremely important for high-current devices. Large beam pipes in the bends appeared to be sufficient to limit the emittance growth even with the holes required to provide an exit path for the laser light.

Next, drift regions at low voltages should be kept as short as possible. Drift regions that are too short, though, would require large velocity modulations and would cause emittance growth because of the mechanism discussed in the previous section. Also, there appears to be an optimum expansion distance for our beam from the gun before we attempt the focusing. The spherical Pierce gun we used was not a good choice for 3-ns pulses. Unless the electronics can be improved to square up the pulse format, the emittance growth can only be reduced by enlarging the beam radius. Planar Pierce guns do this automatically, although they, in general, have higher intrinsic emittances (~40 π·mm·mrad caused by the perhaps four times larger beam). PARMELA runs with a sample planar gun indicated emittances less than 70 π·mm·mrad even out to the end of tank B. Use of a photoelectric injector is the most promising approach because it eliminates all low-voltage drifts [10].

The energy-independent space-charge force could become insignificant if either the emittance is lowered or if the quadrupole triplet Q2 is moved closer to the 60° bend, because this mechanism's effect depends linearly on the beam size. Otherwise, with 400 A, the minimum horizontal emittance after the 60° bend would be about 250 π·mm·mrad; with 800 A, it would be about 350 π·mm·mrad.

We must pay careful attention to the solenoid drift region and special diagnostics should be incorporated. Clearly, each time the beam current is changed, the optimum settings change too (although not linearly with the gun current—a higher amount of bunching can occur with lower total charge).

Finally, note that particle scraping by an aperture would decrease the emittance in a manner that would increase the brightness. Although the emittance growth was mostly restricted to what was originally the bunch's axial ends due to the violent particle overtaking and reordering, scraping off these particles would greatly affect peak current. However computer simulations indicate that brightness increases of a factor of 4 are possible.

Acknowledgment

A large team contributed to the construction and operation of this experiment. In particular, we would like to thank S. Apgar, J. Devenport, J. Hornkohl, C. Humphry, J. Johnson, R. Norris, N. Okay, D. Stephens, and R. Stockley. In addition we would like to thank K. C. D. Chan for several illuminating discussions concerning wake fields.

References

[1] R. True, "The Design of Gridded Pierce Guns for Accelerators," IEEE Trans. Nucl. Sci., 32 (5), 2611 (1985).

[2] M. C. Ross, N. Phinney, G. Quickfall, H. Hoaee, and J. C. Sheppard, "Automated Emittance Measurements in the SLC," 1987 Particle Accelerator Conference, Washington, DC, March 16-19, 1987, to be published.

[3] B. E. Carlsten, "Emittance Growth Caused By Bends in the Los Alamos FEL ERX Beamline," 1987 Particle Accelerator Conference, Washington, DC, March 16-19, 1987, to be published.

[4] R. Warren, "Summary of Measurements of Wakefield Effects," Los Alamos National Laboratory, Accelerator Technology Division memorandum AT-7:87-53, May 1987.

[5] M. E. Jones and B. E. Carlsten, "Space-Charge-Induced Emittance Growth in the Transport of High-Brightness Electron Beams," 1987 Particle Accelerator Conference, Washington, DC, March 16-19, 1987, to be published.

[6] J. Orthel, Boeing Aircraft Company, Seattle, Washington, private communication (1987).

[7] A. H. W. Beck, *Space Charge Waves* (Pergamon Press, New York, 1958).

[8] J. E. Sollid, E. E. Carlsten, D. W. Feldman, and R. W. Warren, "Alignment Techniques Used to Improve Emittance of the Los Alamos Free-Electron Laser," AIAA 19th Fluid Dynamics, Honolulu, Hawaii, June 8-10, 1987, to be published.

[9] P. J. Channell, "Energy Independent Radial Space Charge Forces in Circular Machines," Los Alamos National Laboratory, Accelerator Technology Division Theory Note AT-7:ATN-86-15, April 1986.

[10] B. E. Carlsten and K. C. D. Chan, "Preliminary Injector, Accelerator, and Beamline Design for RF-Linac-Driven XUV Free-Electron Lasers," these proceedings.

FIGURE CAPTIONS

Fig. 1. FEL layout.

Fig. 2. Pulse format from electron gun. Peak current can be increased to 4 A.

Fig 3. Spherical Pierce gun.

Fig. 4. Longitudinal phase space showing effect of velocity modulation and space charge on bunching (10 nC).

Fig. 5. Design of 60° achromatic bend. All edge angles are 17°. Path length in the dipoles is 50 cm.

Fig. 6. Longitudinal phase space diagrams showing bunching effect of nonisochronous bend. Vertical axis is energy (in keV), horizontal axis is phase (in degrees of 1.3 GHz).

Fig. 7. Diagram showing use of quartz screen to determine beam size.

Fig. 8. Around 43% of the particles at the center of the pulse are transmitted through the 4-mm aperture.

Fig. 9. As the current is raised, the beam at location 0 becomes smaller. As a result, the grid pattern seen in the low-current case is destroyed, leaving behind short radial lines at the beam's radial edge.

Fig. 10. Description of beam pipe with hole and choices for steering beam in bend.

Fig. 11. By changing the phase of tank B, we are able to vary the bunch length and peak current of the macropulse at location 5. As the current increases to 400 A, there is a larger and larger spread in the x-dimension, indicating emittance growth.

Fig. 12. Initial beam transverse phase space and shape. Initial beam current density is seen in fig. 2.

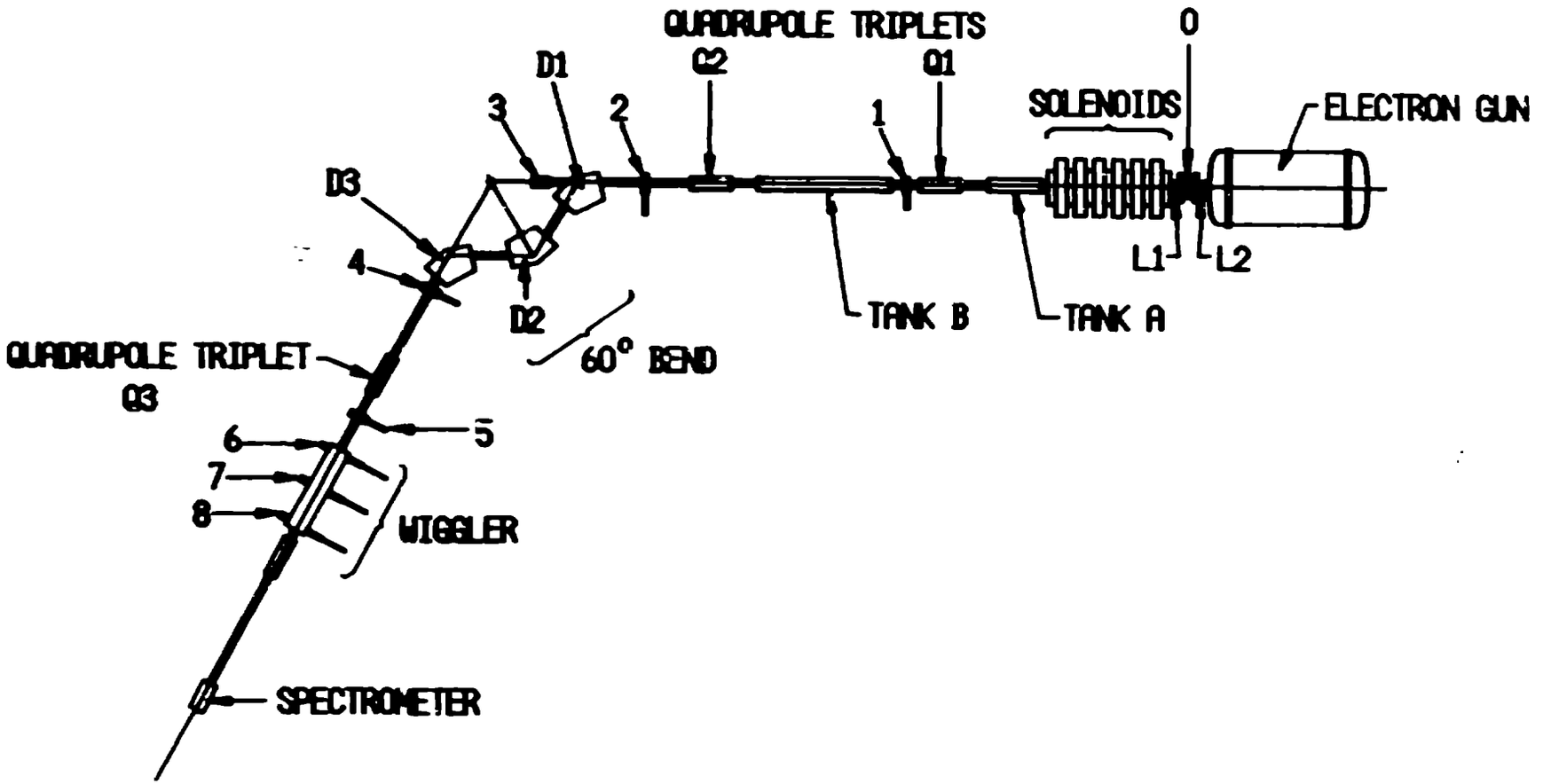
QUADRUPOLE TRIPLETS
Q2
Q1
0
D1
3
2
1
SOLENOIDS
ELECTRON GUN
D3
4
L1
L2
D2
TANK B
TANK A
60° BEND
QUADRUPOLE TRIPLET
Q3
6
5
7
8
WIGGLER
SPECTROMETER

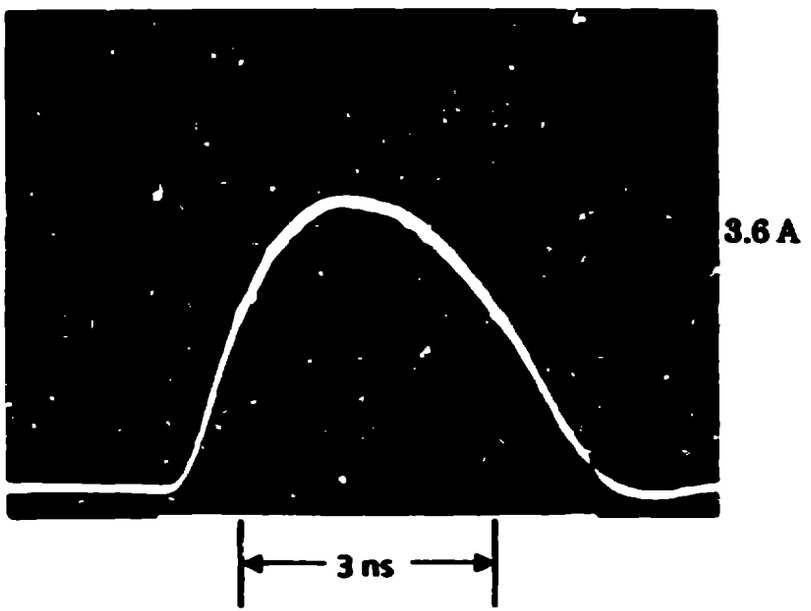
3.6 A
3 ns

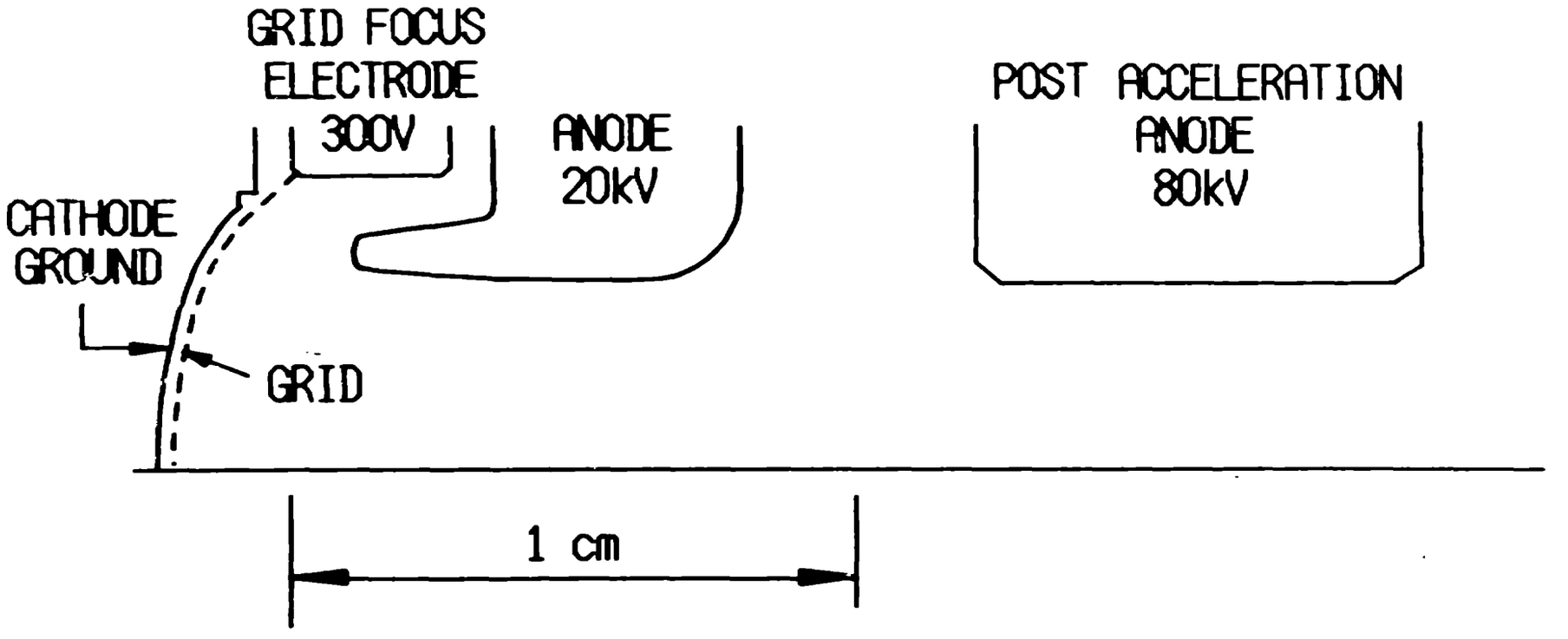
GRID FOCUS
ELECTRODE
300V
ANODE
20kV
POST ACCELERATION
ANODE
80kV
CATHODE
GROUND
GRID
1 cm

Beam Leaving
Subharmonic Buncher

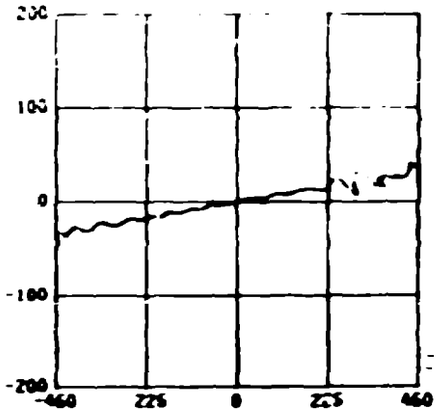

Longitudinal Bunching While Drifting

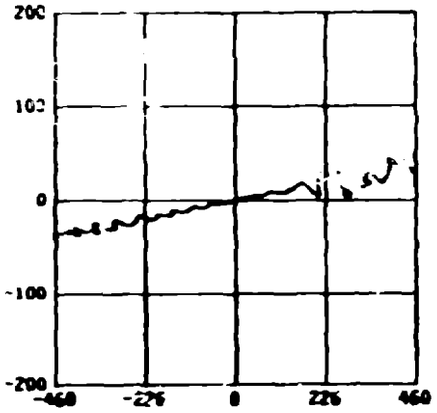

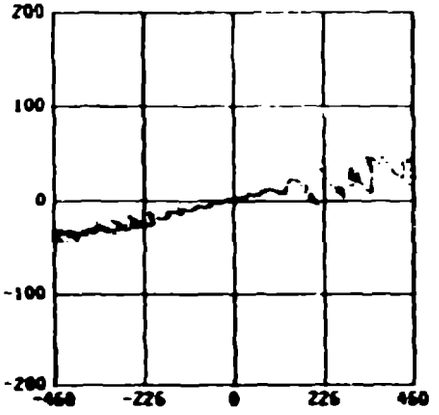

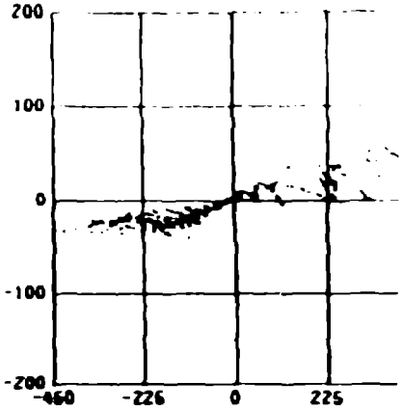

Before Fundamental
Buncher

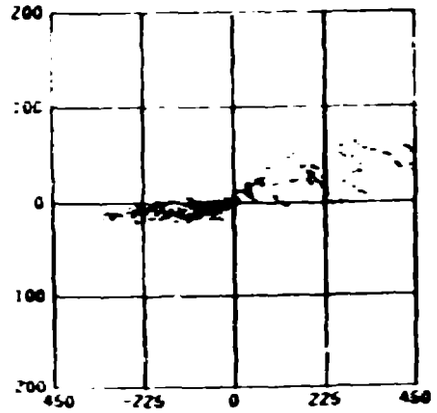

Start of Fundamental
Buncher

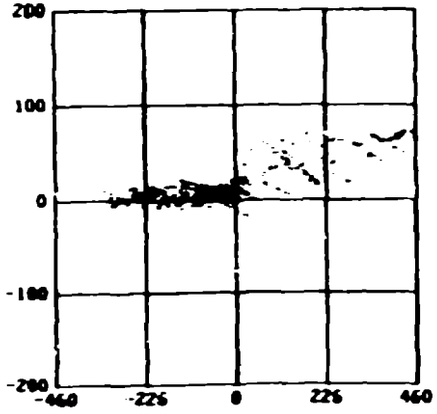

End of Fundamental
Buncher

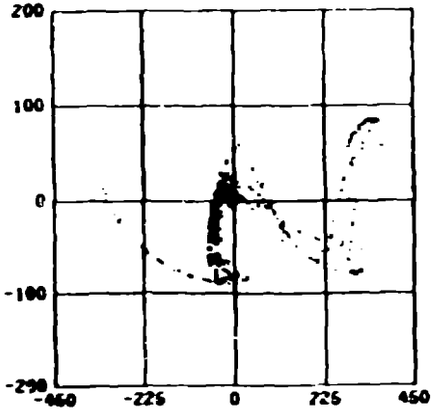

After First Cell
In Tank A

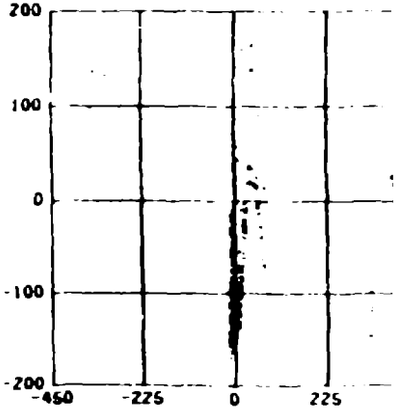

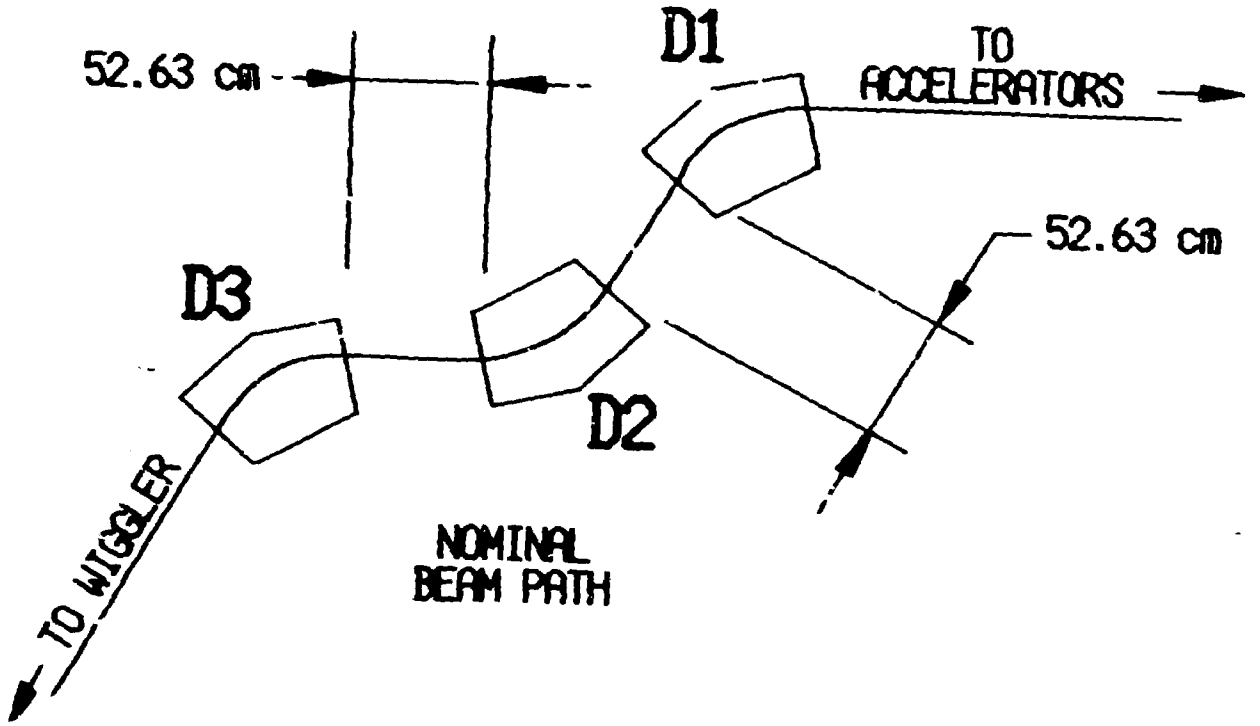
52.63 cm
D1
TO
ACCELERATORS
52.63 cm
D3
D2
TO WIGGLER
NOMINAL
BEAM PATH

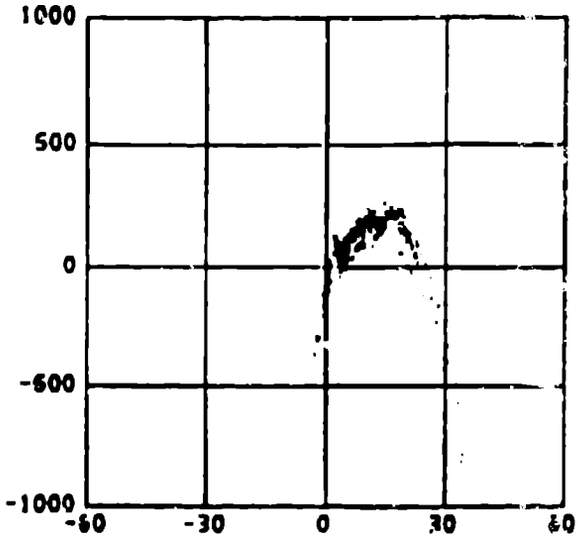

Before Bend

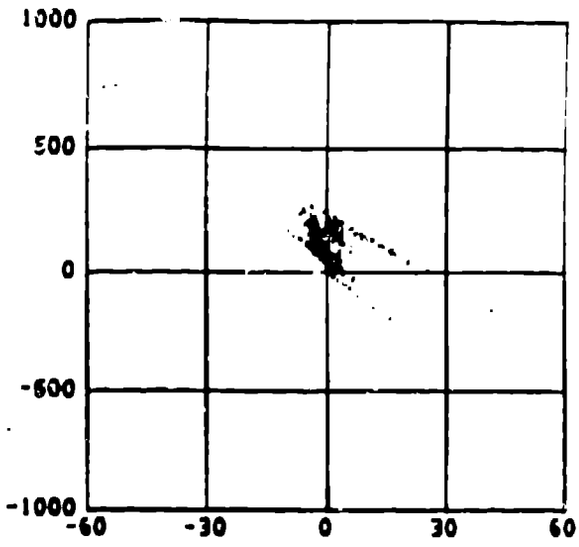

After Bend

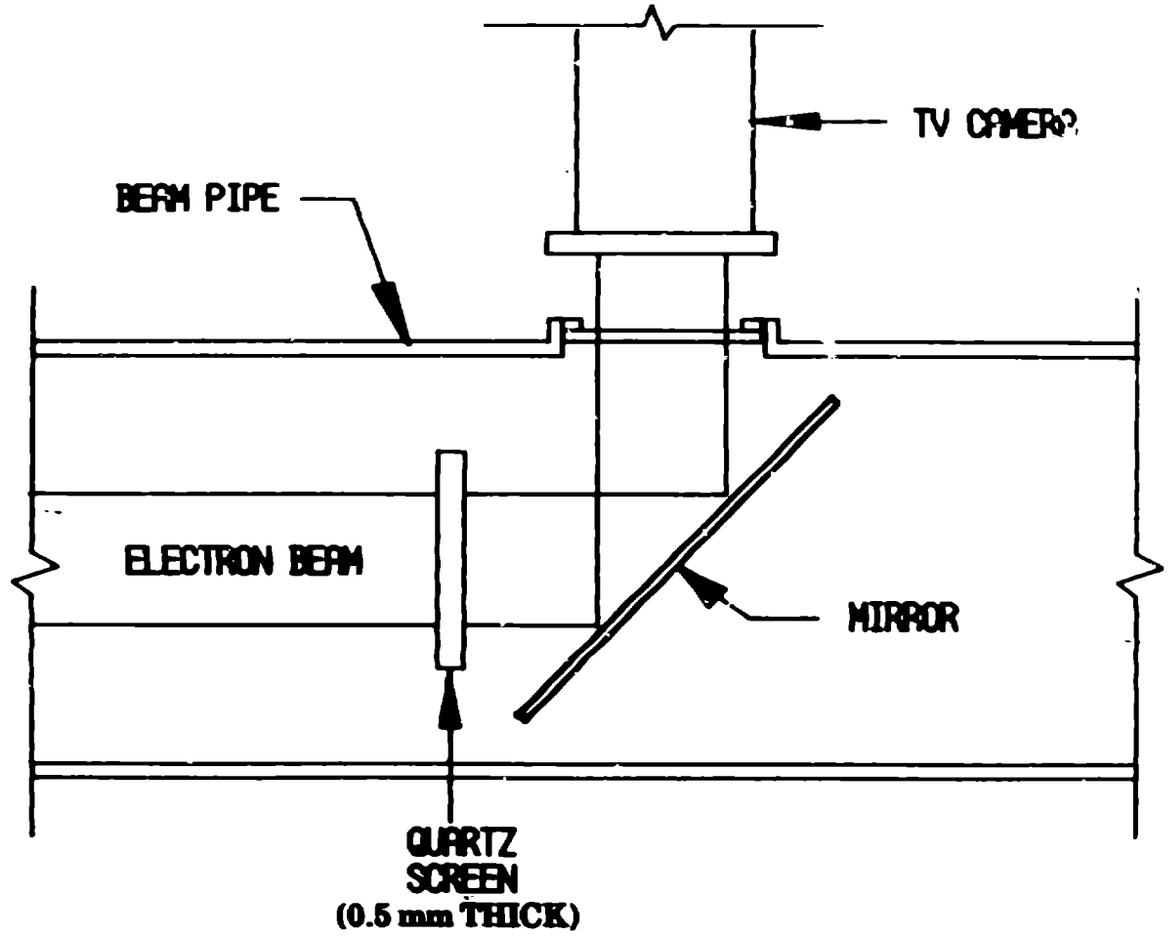
TV CAMERA
BEAM PIPE
ELECTRON BEAM
MIRROR
QUARTZ
SCREEN
(0.5 mm THICK)

4 A

Normal Beam Profile

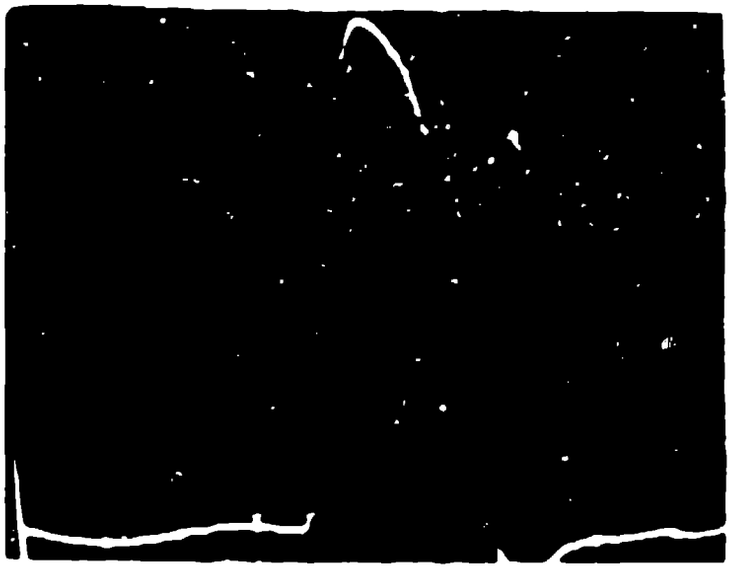

1.7 A

Beam Profile With 4 mm Aperture At Location 0.

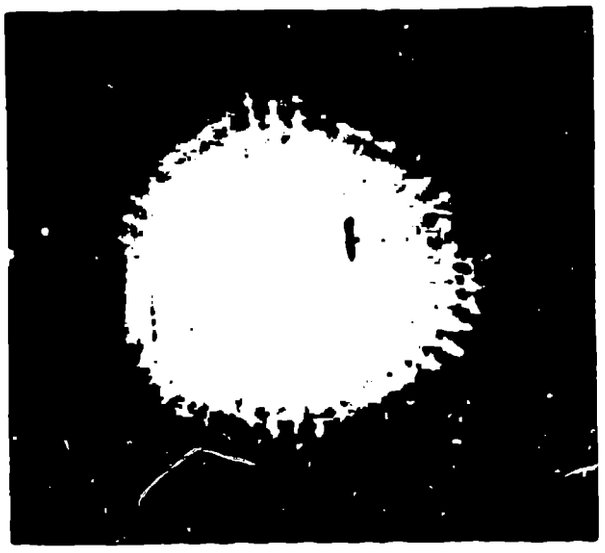

Low Current

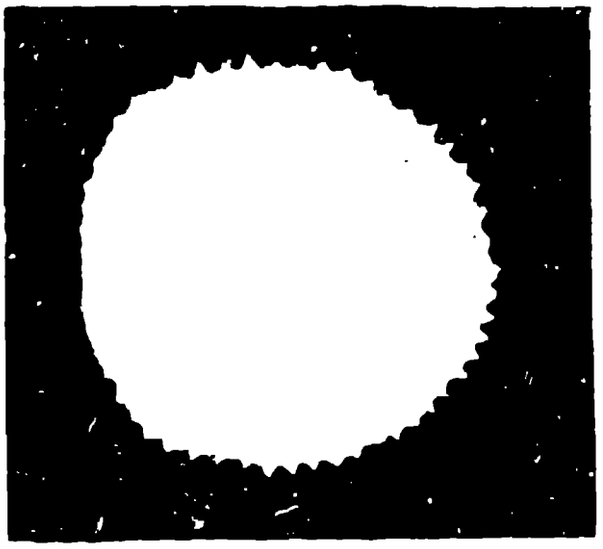

Medium Current

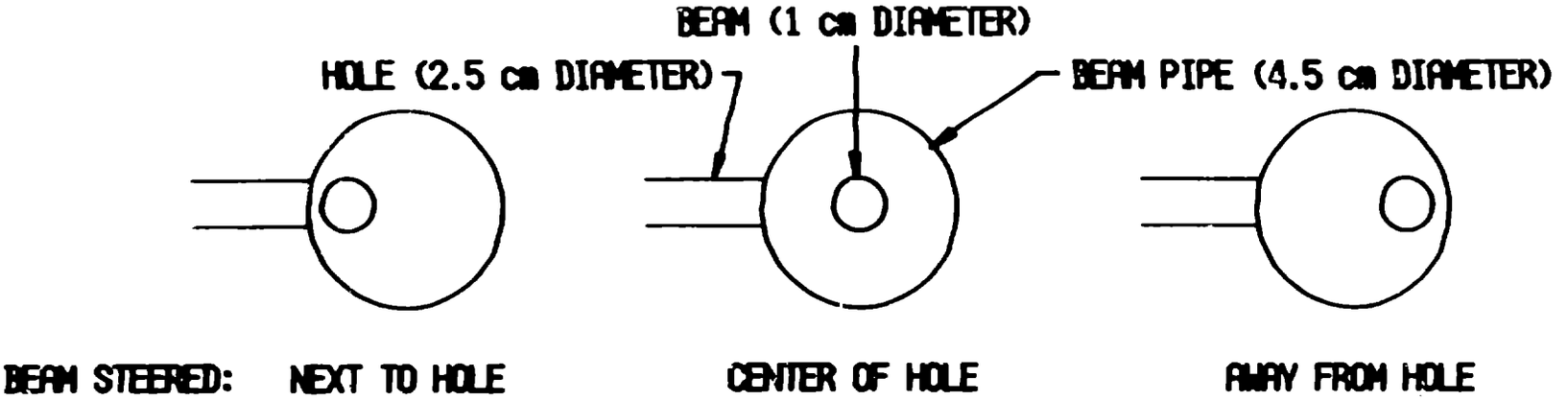

LOOKING ALONG AXIS OF BEAM

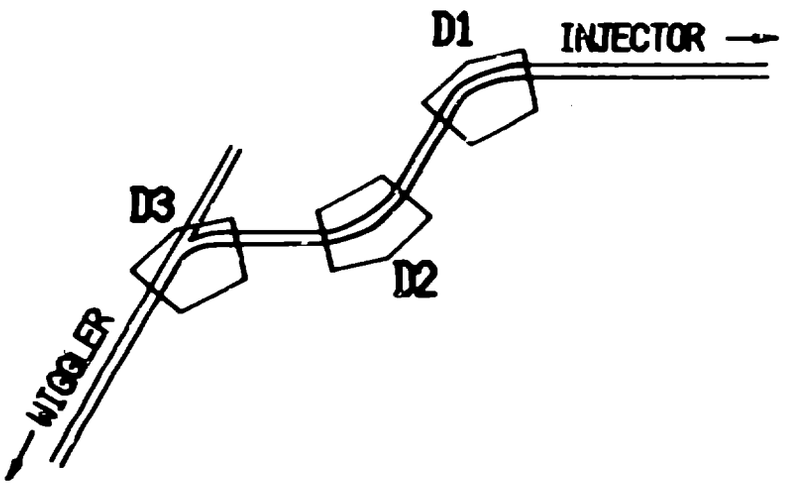

HOLE IN BEAMPIPE IS IN THE THIRD DIPOLE

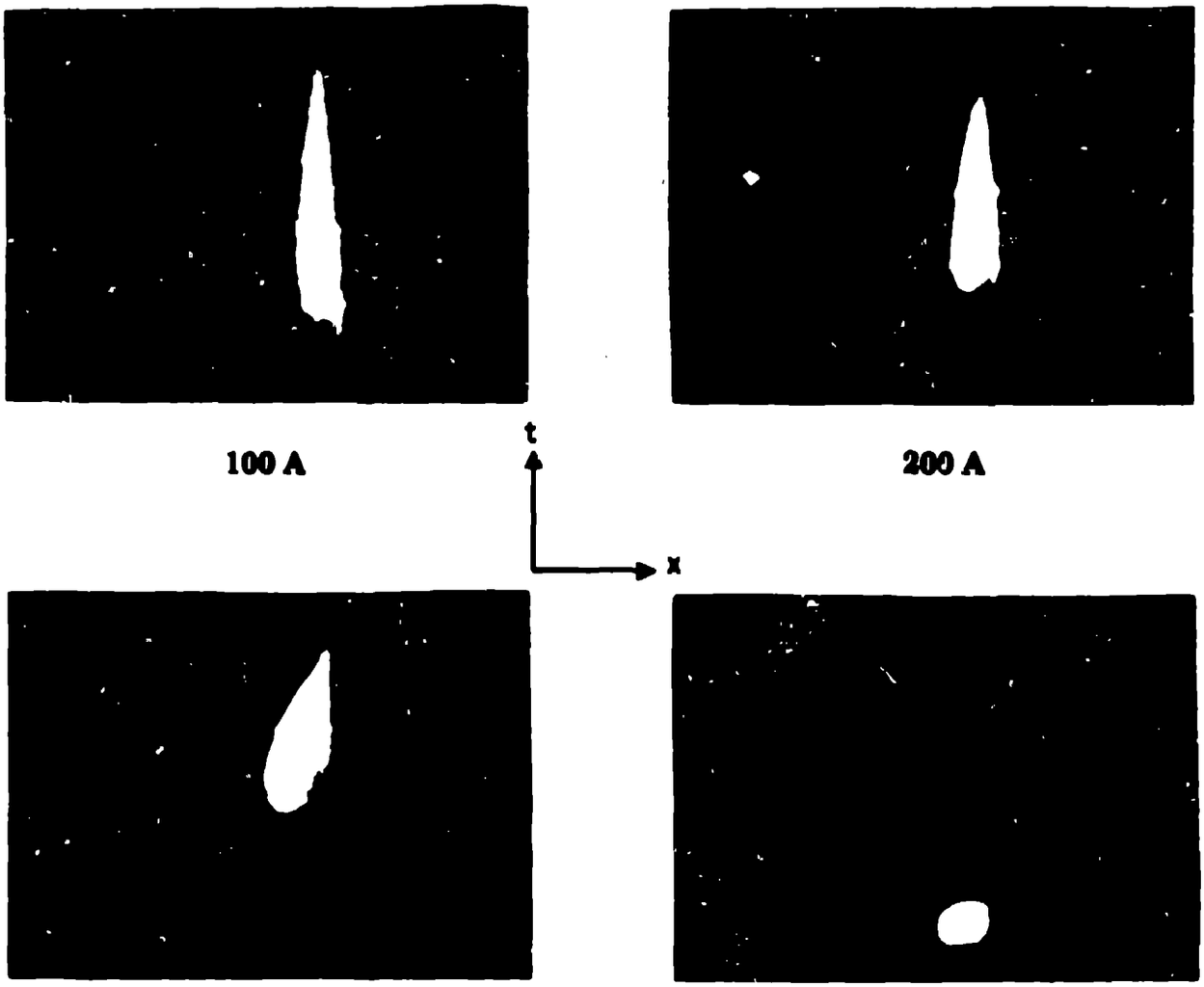
100 A
t
200 A
x
300 A
400 A

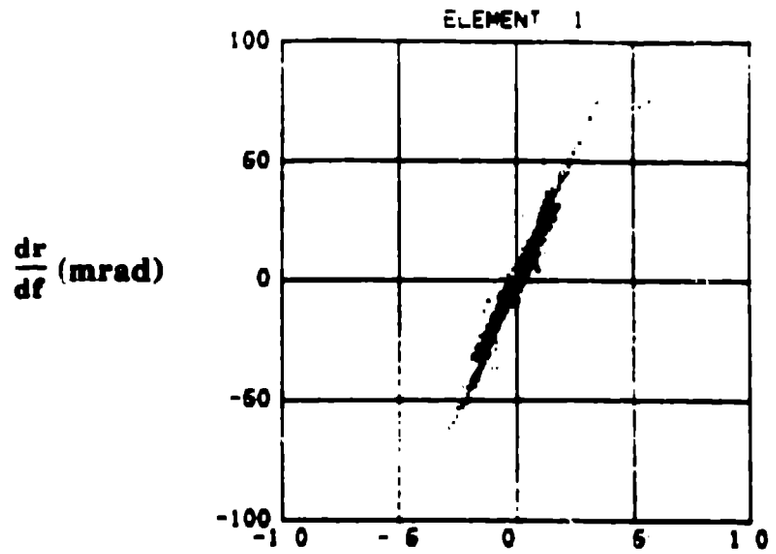

Initial Beam Transverse Phase Space

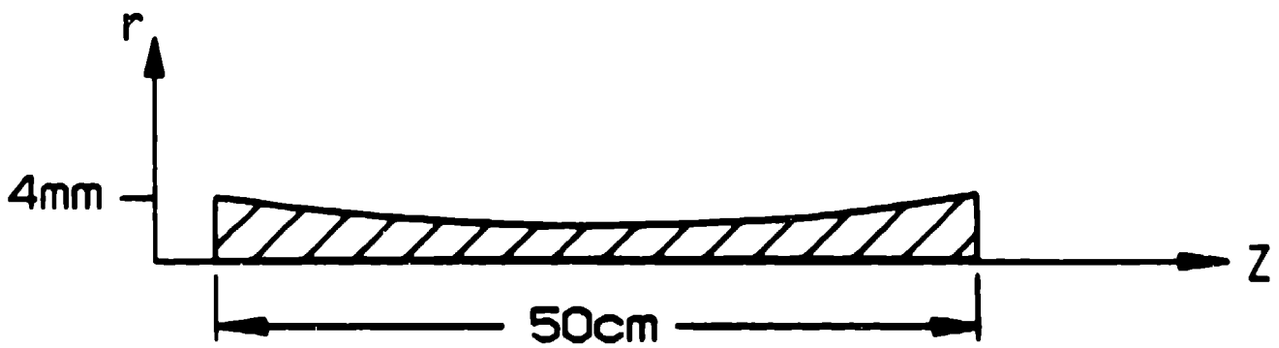

INITIAL BEAM PROFILE